Radiated Power Based on Wave Parameters at Millimeter-wave Frequencies for Integrated Wireless Devices

Damir Senic[1], Kate A. Remley[1], Dylan F. Williams[1], Diogo C. Ribeiro[2], Chih-Ming Wang[1], Christopher L. Holloway[1]

[1]National Institute of Standards and Technology, Boulder, Colorado, USA,
[2]University of Aveiro, Aveiro, Portugal

***Abstract* — We provide total radiated power measurements at millimeter-wave frequencies using a reverberation chamber and a power-calibrated vector network analyzer capable of measuring wave parameters. We compare total radiated power results obtained from two different approaches. In the first approach, applicable when the terminals of the antenna under test are accessible, the total radiated power is calculated directly from forward and reflected waves. In the second approach, when we cannot access the terminals of the antenna under test, the total radiated power is calculated from measured forward and reflected waves at the receive antenna taking into account chamber loss. The results from the two different approaches have excellent agreement, and are within the measurement uncertainty. The uncertainty in our total radiated power measurements is below 2%.**

***Index Terms* — Antenna measurement, communication systems, internet of things, millimeter-wave wireless, reverberation chamber, radiated power measurement, wave parameters, wireless systems.**

I. Introduction

Modern communications systems rely on the modulation of radio-frequency (RF) signals to exchange information. Different equipment can be used to analyze RF signals, including power meters, spectrum analyzers, oscilloscopes, vector signal analyzers, and vector network analyzers (VNAs). Here, we will focus on use of a VNA for analyzing RF signals in terms of total radiated power (TRP).

Power-calibrated VNAs have been traditionally used for conducted power measurements. While this was feasible for devices with accessible output terminals, modern communication devices have integrated antennas and direct measurement at the antenna terminals is not possible. Consequently, the only available solution is a transition from on-wafer to over-the-air (OTA) measurements. Reverberation-chamber-based test methods are efficient, and standardized approaches are recently available for OTA test [1].

Traditionally, reverberation chambers (RCs) were used for various measurements in electromagnetic compatibility (EMC) [2] and, more recently, wireless communications [1]. An RC is an electrically-large resonator with a high-Q value [3], [4]. Due to that fact, the instantaneous spatial distribution of the electromagnetic fields inside such an environment is not uniform. In order to estimate a quantity of interest from measurements in a reverberation chamber, we need to average over measured randomized field samples. Field randomization, or "mode-stirring" techniques include mechanical paddle stirring, where electrically-large paddle(s) move and change the boundary conditions inside a chamber, and position stirring, where the device under test (DUT) antenna is moved.

In this paper, we study total radiated power based on wave-parameter measurements at millimeter-wave frequencies inside an RC. In the past, radiated-emission tests from different RF sources were performed in anechoic chambers or open area test sites, where the limits referred to the maximum electric field strength at certain distance, defined by *e.g.*, [5]. On the other hand, emissions tests performed inside an RC provide us with compliance in terms of TRP. The advantages of using RCs compared to anechoic chambers or open area test sites are mainly in their low cost, simplicity, and shorter measurement times. Much of the prior work on total power radiated by intentional and unintentional sources can be found in [6]-[11].

Wave parameters have the advantage that a power-calibrated VNA can report the forward and reverse waves' power levels directly. By adding a phase reference [12], we can obtain both magnitude and phase information of each frequency component. Even though this paper focuses on TRP from a CW signal, we plan to use the same setup for periodic modulated signals, where a phase reference is of the utmost importance.

Since millimeter-wave frequencies will most likely be used in the next-generation wireless networks [13], we decided to do our research at this frequency range.

II. Radiated Power

According to [2], the amount of RF power radiated (P_{rad}) by a device under test can be determined by measuring the amount of power received by the receive antenna (P_{rec}). Taking into account chamber loss (G_{ref}), P_{rad} can be expressed as:

$$P_{\text{rad}} = \frac{P_{\text{rec}}}{G_{\text{ref}}}. \tag{1}$$

To determine G_{ref} from measurements, we must remove the effects of efficiency and mismatch at the antennas ports. In this case, G_{ref} can be expressed as:

$$G_{\text{ref}} = \frac{\left\langle \left| S_{21} \right|^2 \right\rangle}{\eta_{\text{TX}} \eta_{\text{RX}} \left(1 - \left|\left\langle S_{11} \right\rangle\right|^2\right)\left(1 - \left|\left\langle S_{22} \right\rangle\right|^2\right)}, \tag{2}$$

978-1-5090-4514-3/16/$31.00 ©2016 IEEE

where the brackets denote the ensemble average over the mode-stirring sequence, S_{21} is the forward transmission scattering parameter, and the terms in the denominator represent the free-space radiation efficiency (η_{TX} and η_{RX}) and mismatch for the two antennas. These may be measured in either an anechoic chamber or in an unloaded chamber, such as we have here.

The power at the receive antenna is traditionally measured by a spectrum analyzer, power meter, or base station emulator. In this paper, we will show that power at the receive antenna can be more easily measured by a power-calibrated VNA because all mismatch corrections are performed automatically even while the chamber characteristics are changing. The power will be defined in terms of wave parameters *a* and *b*, where *a* is proportional to the voltage of the incident wave and *b* is proportional to the voltage of the reflected wave at the measurement reference plane, normalized to the square of the system characteristic impedance [14]. In this study, we can access the DUT's antenna terminals. Thus, we can measure the radiated power at the transmit antenna directly in terms of incident (a_1) and reflected (b_1) waves as:

$$P_{\text{rad,direct}} = \left\langle |a_1|^2 - |b_1|^2 \right\rangle \eta_{\text{TX}} . \tag{3}$$

On the other hand, to simulate a DUT whose antenna terminals cannot be accessed, we can also assess total radiated power from (1) by measuring chamber loss (2) and the power at the receive antenna:

$$P_{\text{rad,integrated}} = \frac{P_{\text{rec}}}{G_{\text{ref}}} = \frac{\left\langle |b_2|^2 - |a_2|^2 \right\rangle}{G_{\text{ref}}} , \tag{4}$$

where a_2 and b_2 are wave parameters measured by the VNA at the receive antenna port.

We next describe the measurement setup that we used. In Section IV, we will give the results from (3) and (4) and compare them in order to verify the VNA's applicability for power measurements of wireless devices with integrated antennas.

III. Measurement Setup and Procedures

We performed total radiated power measurements over a frequency range from 43 GHz to 47 GHz using an RC with a power- and phase-calibrated 50 GHz VNA, as shown in Fig. 1. Power was calibrated by a wideband, diode-based power sensor connected to the power meter. Phase calibration was achieved by use of two comb generators, one connected to port 2 of the VNA during the measurements and the other connected to the transmit calibration plane during the calibration of the VNA. Even though a phase calibration is not necessary for total radiated power measurements, we plan to use this setup as a base for more complex, modulated signals measurements where precise phase information of each frequency component is required.

The chamber was equipped with two mechanical stirrers. The larger one rotated about a horizontal (*H*) axis within a cylindrical volume of 0.6 m height and 0.2 m diameter, while the smaller one rotated about a vertical (*V*) axis within a cylindrical volume of 0.5 m height and 0.2 m diameter. The RC's size was 1 m (*l*) × 0.65 m (*w*) × 0.55 m (*h*), which corresponds to an electrical size of approximately 150 λ × 100 λ × 80 λ at the center frequency of 45 GHz.

We used three different transmit antennas that have different radiation patterns (from highly directional to omnidirectional in half-space) to simulate a wide range of real integrated antennas. Measured antennas included a waveguide horn antenna, an open-ended waveguide (OEW), and a microstrip patch antenna. The transmit and receive antennas were oriented away from each other in order to lower the unstirred energy (*K* factor) between them [15]. The RC's bulkhead was equipped with two feedthroughs, one waveguide that was connected to the VNA's port 3 and the other a 2.4 mm coaxial connected to the VNA's port 1. The waveguide horn receive antenna at port 3 was oriented toward the vertical stirrer (see Fig. 1). The signal from the 2.4 mm feedthrough was brought to the transmit antenna via a coaxial cable for the microstrip patch antenna and a coaxial-to-waveguide transition for OEW and waveguide horn antenna.

The transmit antennas were oriented toward the horizontal stirrer and positioned in the middle of the RC's working volume (see Figs. 1 and 2). Key measurement parameters are summarized in Table I.

Wave parameters were measured for 2500 paddle orientations (50 vertical and 50 horizontal). Calibration standards and DUT measurements were collected as raw data, and calibration was performed afterwards within the NIST Microwave Uncertainty Framework [16], [17].

TABLE I: Measurement Parameters

Parameter		Value
Frequency range		43 GHz – 47 GHz
Number of frequency points		1601
IF bandwidth	Calibration	100 Hz
	Measurements	2 kHz
VNA output power level		-10 dBm
VNA dwell time		10 μs
Paddle step size (*V* × *H*)		7.2° × 7.2°
Number of paddle orientations (*V* × *H*)		50 × 50

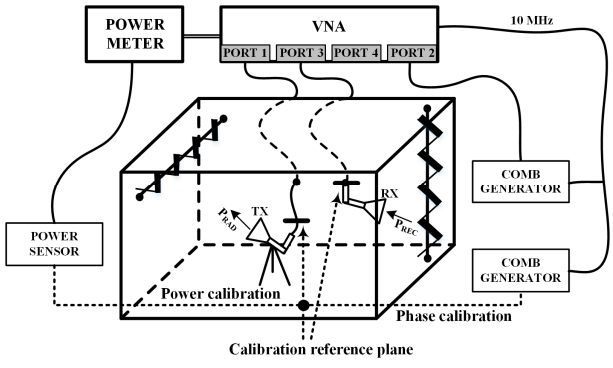

Fig. 1. Schematic layout of measurement setup for total radiated power measurements based on a power- and phase-calibrated VNA.

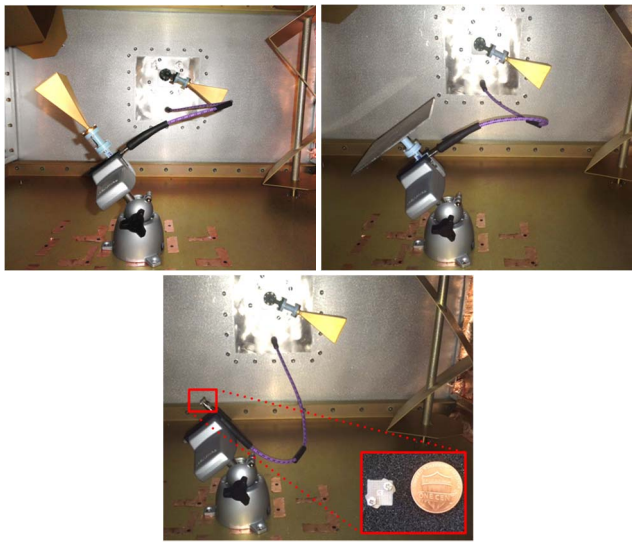

Fig. 2. Three different transmit antennas used for total radiated power measurements; a waveguide horn antenna (top left), an open-ended waveguide (top right), and a microstrip patch antenna (bottom) (compared to a U.S. penny for size).

IV. Results

In this section, we compare total radiated power results measured directly from the wave parameters using (3) to those obtained from scattering-parameters measurements of G_{ref} using (4). We measured G_{ref} with the same pair of antennas we used for our DUT measurements which could artificially lower the uncertainty. Even though these would typically be different pairs of antennas, our focus is on the difference in the approaches from (3) and (4). Note that to calculate the total radiated power by applying (3), we need to have access to the transmit antenna terminals. Common DUTs generally do not have accessible antenna terminals. In that case, we need to use (4). Taking (3) as true value for total radiated power, we will show how good our estimate of total radiated power (4) is based on the received power and chamber loss measurements.

In order to simulate different DUTs, the VNA was connected to various transmit antennas, each with its own radiation pattern and efficiency. The VNA was set to -10 dBm output power. In Fig. 3, we present TRP results for the three different transmit antennas obtained from (3) as solid lines and (4) as dotted lines. The differences in calculated TRP from (3) and (4), given as Δ_{Prad}, are shown in Fig. 4 with error bars as uncertainty values. The mean (over a 4 GHz bandwidth) differences between the two different approaches for the waveguide horn antenna, OEW, and microstrip patch antenna were 0.053 dB, 0.051 dB, and 0.055 dB. Excellent agreement is seen, with differences at or within our measurement uncertainty given in Section V.

Our research indicates that the waveguide horn antenna had the highest average (over 4 GHz bandwidth) TRP of -16.24 dBm. This is due to its high efficiency (low losses and good impedance match). At the same time OEW radiated -16.55 dBm on average, and microstrip patch antenna -17.48 dBm. Note also that the patch TRP drops very fast above 45 GHz. The reason for the drop is poor matching above that frequency. A similar effect was observed in the antenna efficiency study given in [18].

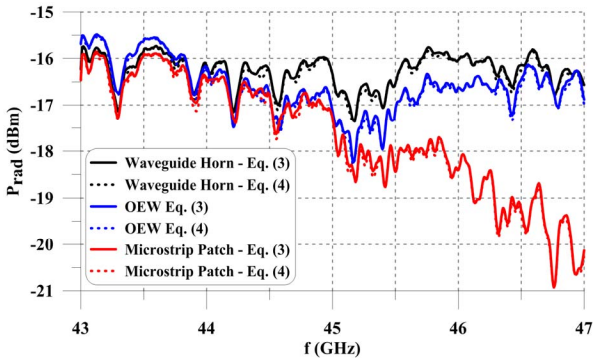

Fig. 3. Total radiated power results calculated from (3) and (4) for three different transmit antennas.

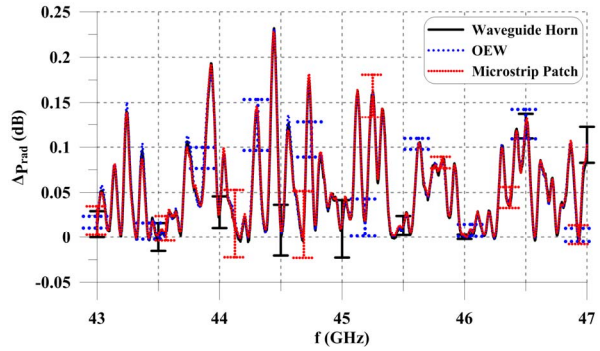

Fig. 4. Differences in TRP results obtained from two different approaches and their associated uncertainties.

V. Measurement Uncertainty

In this section, we provide measurement uncertainty results from the NIST Microwave Uncertainty Framework [16],[17] calculated using both sensitivity and Monte Carlo approaches. The Framework is a NIST-developed software package that allows assignment of uncertainties and probability distributions to error mechanisms in the calibration, and propagates the associated uncertainties to the end result. From repeat measurements, it can also determine random components of measurement uncertainty.

The Framework represents the resulting errors as perturbed measurement vectors that are propagated from one calculation step to the next. This enables uncertainties to be correctly correlated throughout the calculations even when the same uncertainty mechanism is present at different steps of the calculation. The Framework captures and propagates the uncertainties of wave-parameter measurements and finds the correlation between them. By identifying the error mechanisms in the calibration standards, we can determine the correlations between the wave parameters across frequencies, which can then be propagated into the measurement uncertainties.

In [15], [18], we showed that the uncertainty due to the lack of spatial uniformity is not significant for our unloaded chamber. Therefore, we will study only the uncertainty due to the finite number of mode-stirring measurement samples. Regarding future measurements of modulated signals, for which we need to load the chamber to broaden the coherence bandwidth, the uncertainty due to the lack of spatial uniformity should be taken into account.

The uncertainty in the differences between two approaches for the three different simulated DUTs is given in Fig. 4. While the uncertainties for the waveguide horn antenna and the OEW are similar, the higher uncertainty values can be seen for the microstrip patch antenna. The reason for that is caused by the added uncertainty from the de-embedding of a coaxial-to-waveguide adapter. Note that the calibration was performed at the waveguide plane. Maximum uncertainty values from the NIST Microwave Uncertainty Framework for the waveguide horn, OEW, and microstrip patch antennas were 1.75% (0.075 dB), 1.66% (0.071 dB), and 2.41% (0.103 dB).

VI. Conclusion

In this paper, we presented TRP measurement results inside an RC obtained with a power-calibrated VNA at millimeter-wave frequencies. We derived TRP expressions in terms of wave parameters for the two different cases: 1) for accessible DUT antenna terminals, and 2) for integrated DUT antennas. In the first case, the TRP can be easily calculated by measuring power levels of forward and reflected waves. In the second case, besides measuring power levels of forward and reflected waves at the receive antenna, we also need to measure the chamber loss. Results obtained from the two different approaches were compared and showed excellent agreement within our calculated measurement uncertainties.

We performed measurement uncertainty analysis using the Microwave Uncertainty Framework, which assigns uncertainties and probability distributions to error mechanisms in the calibration, and propagates the associated uncertainties to the end result. The uncertainties we obtained agree well with uncertainty calculations in our previous research employing an unloaded RC.

Here, we showed that a power-calibrated VNA extended existing methods for radiated power measurements. Our future work will include TRP measurements of modulated signals at millimeter-wave frequencies based on an RC and power- and phase-calibrated VNA.

Acknowledgement

The authors would like to thank to Michael D. Janezic of the NIST National Advanced Spectrum and Communications Test Network (NASCTN) who provided us with a precision WR22 calibration kit needed for our measurements.

References

[1] CTIA Certification, “Test Plan for Wireless Large-Form-Factor Device Over-the-Air Performance” Sep. 2016.

[2] “IEC 61000-4-21: EMC, Part 4: Testing and Measurement Techniques; Section 21: Reverberation Chamber Test Methods,” Int. Electrotech. Comm., Geneva, 2011.

[3] D. A. Hill, “Electromagnetic theory of reverberation chambers,” U.S. National Institute of Standards and Technology Technical Note 1506, 1998.

[4] D. Kajfez, *Q factor*, Oxford: MS: Vector Fields, 1994.

[5] “IEC 61000-4-22: EMC, Part 4: Testing and Measurement Techniques; Section 22: Radiated emissions and immunity measurements in fully anechoic rooms (FARs),” *Int. Electrotech. Comm.*, Geneva, 2010.

[6] P. Corona, G. Latmiral, E. Paolini, and L. Piccioli, “Use of reverberating enclosure for measurements of radiated power in the microwave range,” *IEEE Trans. Electromagn. Compat.*, vol. 18, no. 2, pp. 54–59, May 1976.

[7] D. A. Hill, D. G. Camell, K. H. Cavcey, and G. H. Koepke, “Radiated emissions and immunity of microstrip transmission lines: theory and reverberation chamber measurements,” *IEEE Trans. Electromagn. Compat.*, vol. 38, no. 2, pp. 165–172, May 1996.

[8] M. B. Slocum and M. O. Hatfield, “Evaluation of proposed IEC reverberation chamber methodology for radiated emissions measurements using a reference radiator,” in *IEEE Int. Symp. Electromagn. Compat.*, pp. 734–739, Aug. 13–17, 2001.

[9] H. G. Krauthäuser, “On the measurement of total radiated power in uncalibrated reverberation chambers,” *IEEE Trans. Electromagn. Compat.*, vol. 49, no. 2, pp. 270–279, May 2007.

[10] C. Orlenius, P. Lioliou, M. Franzén, and P-.S. Kildal, “Measurements of total radiated power of UMTS phones in reverberation chamber,” in *European Conference on Antennas Propag., EuCAP*, Nov. 11–16, 2007.

[11] V. Monebhurrun, T. Letertre, “Total radiated power measurements of WiFi devices using a compact reverberation chamber,” in *IEEE Int. Symp. Electromagn. Compat.*, Jan. 12–16, 2009.

[12] P. Roblin, *Nonlinear RF circuits and nonlinear vector network analyzers*, New York: Cambridge University Press, 2011.

[13] T. S. Rappaport, S. Sun, R. Mayzus, H. Zhao, Y. Azar, K. Wang, G. N. Wong, J. K. Schulz, M. Samimi, and F. Gutierrez, ‘‘Millimeter wave mobile communications for 5G cellular: It will work!,’’ *IEEE Access*, vol. 1, pp. 335–349, 2013.

[14] Keysight Technologies Application Note 5988-9215EN, “Fundamentals of RF and microwave power measurements (Part 3),” USA, August 1, 2014.

[15] D. Senic, K. A. Remley, C.-M. Wang, D. F. Williams, C. L. Holloway, D. C. Ribeiro, and A. T. Kirk, “Estimating and reducing uncertainty in reverberation-chamber characterization at millimeter-wave frequencies,” *IEEE Trans. Antennas and Propag*., vol. 64, no. 7, pp. 3130–3140, Jul. 2016.

[16] D. F. Williams, NIST Microwave Uncertainty Framework, Beta Version. NIST, Boulder, CO, USA, Jun. 2014. Available online: https://www.nist.gov/services-resources/software/wafer-calibration-software

[17] J. A. Jargon, D. F. Williams, T. M. Wallis, D. X. LeGolvan, and P. D. Hale, “Establishing traceability of an electronic calibration unit using the NIST Microwave Uncertainty Framework,” in *79th ARFTG Conf. Dig*, Montreal, QC, Canada, Jun. 2012, pp. 32–36.

[18] D. Senic, D. F. Williams, K. A. Remley, C.-M. Wang, C. L. Holloway, Z. Yang, and K. F. Warnick, “Improved antenna efficiency measurement uncertainty in a reverberation chamber at millimeter-wave frequencies,” *IEEE Trans. Antennas Propag*., IN PROCESS